MANCHESTER 1824
The University of Manchester

Classification of Non-ferrous Metals using MIS

Third Year Individual Project – Final Report

May 2022

Ahmad Huneiti

10528746

Supervisor: Professor Anthony Peyton

School of Electrical and Electronic Engineering

Contents

Total word count: 7753

Abstract

Nowadays, new and advanced sorting methods are being introduced at an increasing rate. This growth is due to the fact that countries and leaders around the world are starting to realize the adverse effects of global warming. In an effort to reduce such effects, the majority of countries around the world have vowed to reduce their carbon footprint. An essential way of reducing the total greenhouse gas emissions is by reducing the number of raw materials that are being extracted from the earth's core. This can be done by recycling and reusing materials. Therefore, as recycling increases, it is important to be able to sort and recycle materials efficiently and safely. One of the most recycled materials is non-ferrous metals. These metals are mostly recovered by hand whereby a worker identifies the metal based on its physical appearance. This method of sortation is neither efficient nor safe. This paper investigates a new method of scrap sorting, known as Magnetic Induction Spectroscopy (MIS), that identifies non-ferrous metals based on their respective magnetic induction spectra. This method increases efficiency and reduces the costs associated with sorting as the number of workers is reduced. Moreover, if this method is implemented in factories, it will significantly reduce the health risks posed by hazardous wastes and accidents. Although this new method of sortation has great potential, it still has some limitations that must be overcome. One major limitation is the low recovery rate.

1. Introduction

Non-ferrous metals are being used in various industries such as transport, aerospace, construction, and electricity. Some of the most commonly used metals are Aluminium and Copper because of their low weight and high conductivity respectively (Non-ferrous metals). As opposed to having such useful metals thrown away in landfills, it would be significantly more beneficial to recycle them. Not only would that help protect our planet, it would also preserve natural resources. Also, by recycling scrap aluminium only 5% of the energy needed to produce virgin aluminium is required (Beason, 2019). As a result, the production of aluminium from scrap between 2000 and 2015 has increased by 86% (BIR - Non-Ferrous Metals, 2020). During recycling the non-ferrous metals have to be sorted and extracted from scrap which includes a mixture of shredded non-ferrous metals usually referred to as Zorba. Currently, the most common method of sortation is hand sorting whereby people inspect the scrap and distinguish the non-ferrous metals from other metals by inspecting their characteristics. However, this method is inefficient as it is time-consuming and labour-intensive. A much more advanced and accurate method is the use of sensors that can measure the different properties of each material and then based on the properties the metals are classified accordingly.

Nowadays different types of sensors are being used to develop sorting systems. For example, in a system that uses Laser Induced Breakdown Spectroscopy (LIBS) a laser beam emitted onto the sample causes a small volume of the sample mass to be ablated. At this point, the ablated mass is highly energetic and a plasma is formed as a result of interacting with the laser. The plasma then cools and emits light with distinct spectral peaks that are collected and analysed to determine the major elements in the sample (Russo, R., et al., 1999). Another example of a sensor-based system includes the use of X-Ray Fluorescence (XRF). When X-ray is absorbed by an element nearly all elements fluoresce as a result of excitation. XRF analysers generate this excitation and then capture the fluorescence that is emitted by the elements (Scrap Recycling with XRF – Sort More, Sort Faster, and Increase Your Profits). The captured fluorescence is then compared with a set threshold to identify the material that is being examined. Both the LIBS and XRF have proven to be accurate and efficient techniques used in scrap sorting; however, for basic sorting the increased costs and complexity associated with such sophisticated technologies makes it difficult to be used in underdeveloped countries where cost is a major factor to consider.

The aim of this report is to further progress the metal sorting industry by developing a sensor-

based system that is able to classify the different classes of non-ferrous metals and address the increased costs associated with such systems using Magnetic Induction Spectroscopy (MIS). For MIS, a magnetic field is used to induce eddy currents across the sample which generates a secondary magnetic field that is measured by a receiver coil. The impedance of the sample then affects the magnitude and phase of the secondary magnetic field resulting in an impedance spectrum that can be analysed to determine the material under test (O'Toole, M., et al., 2015). By using a 3D shape scanner, we will be able to scan the different materials and input the results into a computer simulation which will later allow us to compare our simulated measurements with the true values. For this project, Ansys Maxwell will be used to induce eddy currents across the different samples that will be tested throughout the project. However, to input the samples scanned by the shape scanner into Maxwell an intermediary software known as FreeCAD will be used to convert the files acquired by the scanner into STEP files.

The report goes through extensive research regarding the use of MIS in sorting systems. The research includes details about how such systems may be able to differentiate and classify the metals as well as the limitations associated. The report then provides a detailed explanation of the methodology used in the project. Finally, the results obtained by using the softwares mentioned above are analysed and discussed thoroughly.

Starting with chapter 2, the report explains how the world is moving towards a more sustainable society as the effects of climate change unravel and highlights the importance of investing in carbon free technologies. Chapters 3 and 4 then cover the theory behind magnetic induction spectroscopy and thoroughly explain the set up that was used to test this theory. Moreover, the results that were obtained during the research are analysed and discussed in chapter 5. Finally, chapter 6 concludes the report and includes some further work that may help improve the MIS system's recovery rate.

2. Literature review

2.1. Environmental impact

The extraction of the most common non-ferrous metals involves smelting which is a process whereby the metal is extracted by heating and melting its ore. For example, the production of aluminium from its ore (bauxite) involves refining bauxite to obtain alumina followed by smelting alumina to get the final product known as aluminium. However, due to the high stability of bauxite, large amounts of electricity are required during the smelting process, which as a result means that large quantities of coal are burnt. It is estimated that the production of aluminium accounts for 1.1 billion tonnes of carbon dioxide (a greenhouse gas that contributes to global warming) emissions per year which translates to about 2% of global human-caused emissions (Van Heusden, R., et al., 2020). Nonetheless, since aluminium is an essential material in several industries such as construction, transportation, and electrical products, the demand for aluminium will continue to increase in the future. Therefore, it is vital to address the emissions caused by aluminium and other non-ferrous metals as well. As of June 2019, the UK became the first major economy to pass laws to reduce its emissions to net-zero by 2050. This is part of its pledge to The Paris Agreement, a legally binding international treaty with the goal of containing the global temperature increase under 2 degrees Celsius.

Since the passing of these laws, there has been a significant decrease of almost 615% of carbon monoxide emissions in the UK between 2005 and 2019. Emissions dropped from 3.9 million metric tons in 2005 to 545,000 metric tons in 2019 (UK: aluminum production CO2 emissions 1990-2019 | Statista, 2021). This decrease can be contributed to the switch from primary production to secondary production of aluminium, which refers to the recycling of scrap to form new products. The continual rise in energy prices and the recent commitments made by the UK government to reduce emissions has placed significant pressures on the production of non-ferrous metals especially with the increased demand for such metals. At the current rate, the UK is still not on track to meet its target of net zero carbon emissions by 2050. In June 2021, a progress report that highlights the actions and strategies that will be taken by the UK's government was published by the committee on climate change (CCC). The report states that for the UK to get on the path of net zero emissions, it must make lasting reductions in emissions. Examples to achieve this include encouraging the sale of electric vehicles, the deployment of supporting charging infrastructure, as well as the deployment of renewable electricity generation (Climate Change Committee, 2021).

2.2. The role of non-ferrous metals

It is expected that the demand for non-ferrous metals will increase as the world starts to transition from the use of gasoline vehicles to electric vehicles. As the transition occurs, studies show that the global electric vehicle market is expected to increase by a compound annual growth rate of 14.1% between 2019 and 2030 (Global battery electric vehicle market size forecast 2030 | Statista, 2022). This growth in electric vehicles has had a significant impact on non-ferrous metals as car manufacturers now seek the use of lighter yet stronger metals such as lithium and cobalt. Another non-ferrous metal which has experienced increased demand due to the introduction of electric vehicles is copper. According to the Copper Development Association (CDA), a conventional car uses only 18 to 49 lbs of copper compared to the 183 lbs of copper used in electric cars (Copper Development Association, 2022). Unlike the conventional gasoline car that makes use of an internal combustion engine, most electric cars make use of an induction motor that transforms electricity into mechanical energy to move the car. An induction motor consists of a stationary portion known as the stator and a rotating portion known as the rotor that is fixed to the motor shaft. As the copper wound stator is energized from the power supply, a rotating magnetic field is produced that in turn provides an electromotive force that produces a moving torque at the rotor. This suggests that copper is an essential part of the motors that are used to produce electric vehicles. As a result, it is expected that the demand for copper due to electric vehicles will increase by 1,700 kilotons by 2027 (Copper Development Association, 2022).

As part of the Paris Agreement, numerous countries have already started to invest in low-carbon energy technologies to help in the sustainable transition. Such technologies include the deployment of renewable energy systems such as solar and wind energy. However, the main challenge is that the technologies associated with such systems require much more material than the traditional systems based on fossil fuels. For example, in wind turbines the two mostly used designs are either the geared turbines, which include a gearbox that requires a significant amount of copper or a direct-drive turbine which consists of permanent magnets containing rare earth metals (Arrobas, D., et al., 2017). As for solar systems, the dominating technology for constructing solar photovoltaic cells is the crystalline silicon cells which consist of aluminium, lead, and nickel. Crystalline silicon cells currently make up about 85% of the market (Arrobas, D., et al., 2017).

It is evident that as the world transitions to a sustainable and low-carbon environment, the demand for non-ferrous metals will increase. Consequently, it is vital to make sure that enough supply is continuously available and that the metals are produced in a sustainable manner which

will allow for countries to meet the commitments made in the Paris Agreement. For this to happen, a circular economy must be implemented whereby non-ferrous metals are recycled in a closed loop process. Closed-loop recycling refers to the process by which scrap is collected and then recycled to produce the same or a new product. This method of recycling has proven to be exceedingly efficient. As a matter of fact, the 2021 Nissan Rogue has been built using a closed-loop recycling process for aluminium parts.

To achieve such efficient recycling systems, the scrap must be sorted properly. At the present time, the most common method of sortation is hand-sorting by which workers handpick and sort the metals based on their physical characteristics such as appearance, colour, and conductivity. This reduces the efficiency of the process as it poses the risk of human error, and more importantly, it may threaten the workers' health due to the exposure to hazardous waste. Some of the health and safety risks faced by workers in sorting and recycling facilities include:

1. Exposure to harmful substances: This refers to sharp objects that may injure workers and toxic chemicals. For example, mercury that may be found in batteries and televisions can produce harmful effects if inhaled by workers.

2. Moving vehicles: Due to the heavy materials that are found in these facilities forklifts and trucks are used to transport them. This increases the risk of workers being struck by moving vehicles which may result in fatal injuries.

3. Slips and trips: It is common for workers in such workplaces to experience these risks caused by obstructions in walkways and poor floor specifications.

All the mentioned risks have been mitigated by providing the necessary and appropriate policies. These policies and regulations are set by governmental agencies to ensure that employers provide a safe and healthy working environment for their employees. Yet, this is not necessarily the case for workers in underdeveloped countries where their well-being is not monitored and there are no labour unions to represent the interests of the workers.

In order to reduce the weaknesses associated with hand-sorting, automated systems that distinguish between metals using sensors have been developed. The most advanced and accurate sensors currently being used are the LIBS and XRF sensors. As a new and emerging technology, LIBS has gained popularity and is establishing itself as a tool for identifying different metals alongside XRF. Both techniques have proven to be reliable and accurate. Nonetheless, there are some limitations associated with the use of XRF and LIBS to identify unknown samples of metals.

As previously discussed, the XRF analysers capture the fluorescence that is emitted by the sample being tested. The energy of the fluorescent X-rays is dependent on the atomic number of the element. Therefore, light elements that have low energy levels will produce X-rays that may not be able to penetrate the air and reach the analyser. Even if the X-rays reach the analyser, an insignificant amount will be identified by the detector making it difficult to recognize the type of metal (Tykot, 2016). As a result, light elements such as Beryllium and Lithium cannot be detected using XRF technology. The main challenge with LIBS is that it is not yet ready to be deployed in industrial facilities as more research and development is required to make it compete with existing technologies. Also, at the present time, XRF provides a higher accuracy when compared to LIBS. Alongside the challenges mentioned, both XRF and LIBS also require a costly and complex set-up to achieve accurate analysis which makes it difficult to implement such technologies in facilities that require low-cost and relatively easy to use systems.

In this paper, we propose the use of MIS sensors to develop affordable and accurate systems that are able identify metals and that can be deployed in underdeveloped countries to replace the hand-sorting methods that are currently being used.

2.3. Magnetic induction spectroscopy

Magnetic induction refers to the process by which an object becomes magnetized due to an external magnetic field. The idea of magnetic induction was first discovered by Michael Faraday in 1831. Later on, James Clerk Maxwell further developed Faraday's discovery into a mathematical equation known as the Maxwell-Faraday equation. The equation states that a time-varying magnetic field always accompanies a spatially varying non-conservative magnetic field, and vice versa. The equation is

$$\nabla \times \mathbf{E} = -\frac{\partial \mathbf{B}}{\partial t}, \tag{1}$$

where ∇ is the curl operator, **E** is the electric field, and **B** is the magnetic field.

In this report, we attempt to investigate a method which is based on MIS where as a result of the generated secondary magnetic field we are able to plot the impedance spectrum for different metals. The main challenge with MIS is that in some applications the information provided is not sufficient and therefore making it an impractical solution. This problem may be overcome by combining the MIS system with a camera and colour scanner. This combination allows the system to scan the shapes and colours of the metals before identifying them which results in higher

recovery rates. Unlike LIBS, MIS is considered to be a non-destructive analytical technique which means it does not alter the chemistry of the metal under test. When compared with the traditional sorting methods, the implementation of MIS techniques can result in significant benefits. These include:

- Increase in the safety levels of sorting.
- Reducing injury rates by eliminating dangerous jobs such as exposure to harmful substances.
- No moving or mechanical parts which reduces the need of maintenance and repair.
- Reduced costs and increased efficiency of sorting as the number of workers is reduced.
- No laser or radiation involved which reduces the risk of injury.
- Unaffected by dirt or contaminants.

3. Theory

When current is induced in a primary coil (Tx), a magnetic field is generated. If an electrical conductor such as a metal is exposed to the generated magnetic field, eddy currents will be induced inside the exposed metal. The eddy currents tend to oppose the original magnetic field and therefore a secondary magnetic field is created in the opposite direction. This secondary magnetic field can then be measured by a receive coil (Rx) and the electromagnetic properties of the metal are reflected in the receive coil (Dingley, G. and Soleimani, M., 2021). The schematic below provides an illustration of process.

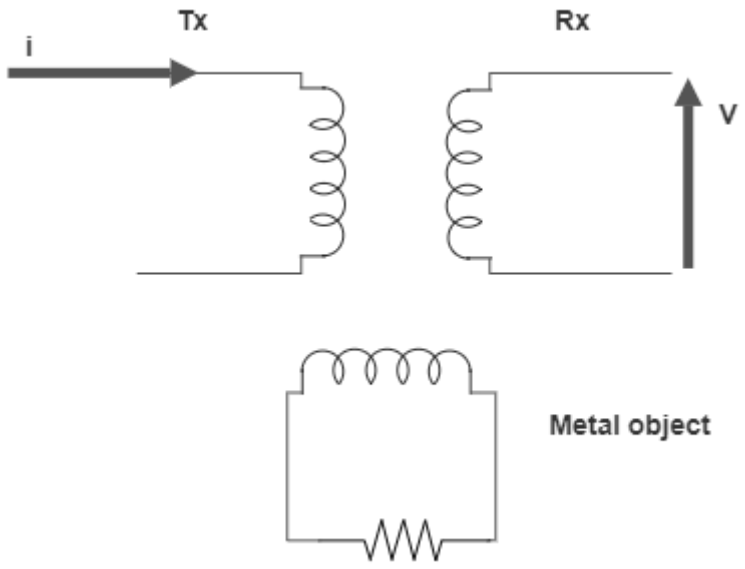

Figure 1. Circuit equivalent of primary coil, receive coil, and metal object.

The total impedance Z_T is then calculated as the ratio of voltage and current:

$$\mathrm{Z_T} = \frac{\mathbf{V_{Rx}}}{\mathbf{i_{Tx}}} = \mathrm{R} + \mathrm{j}\omega\mathrm{L}\ , \tag{2}$$

Where R is the resistance of the metal object and L is the inductance of either the primary coil (Tx) or the receive coil (Rx). It does not matter which inductance is chosen as both are the same ($\mathrm{L_{Tx}} = \mathrm{L_{Rx}} = \mathrm{L}$). ω is the corresponding angular frequency.

The voltage $\mathrm{V_{Rx}}$ produced in the receive coil is a result of the change in current in the primary coil, this effect is known as mutual inductance. The mutual inductance M can be defined as the proportionality between the voltage generated in the receive coil to the change in current in the primary coil.

$$\mathrm{M}(\mathrm{j}\omega) = \frac{\mathrm{Z_T}}{\mathrm{j}\omega} = \frac{\mathrm{R}}{\mathrm{j}\omega} + \mathrm{L} = \mathrm{M}'(\omega) + \mathrm{jM}''(\omega)\ , \tag{3}$$

Where M' and M'' refer to the real component and imaginary component of the mutual inductance at a frequency ω respectively.

The magnetic induction spectrum of a metal fragment is plotted using the real and imaginary components of the mutual inductance. The typical shape of the real component for a non-ferrous metal is a sigmoid starting at zero that converges to an asymptote as the frequency increases. The imaginary component shows a curve that starts at zero and then reaches an extremum before converging back to zero (D. O'Toole, M. and J. Peyton, A., 2019).

Different metals are classified by their unique magnetic induction spectra which is explained by the skin-depth effect. Skin-depth refers to the non-uniform distribution of current in a conductor. At higher frequencies, the eddy currents tend to flow in a thin layer near the surface of the conductor and away from the centre. This explains why the real component of the mutual inductance converges to an asymptote. Skin depth is dependent on the frequency, conductivity, and permeability of the material. Thus, different materials will produce different curves in the magnetic induction spectra allowing us to classify the different metals based on the shapes of their real and imaginary components.

4. Methodology

4.1. Digital twin

The central principle underlying this research is to create a digital twin of the scanning system. A digital twin refers to a virtual representation that is designed to accurately reflect a physical object or process. In the context of this project, the metals are the physical objects that will be scanned using a 3D scanner. The scans will then be used to create a digital model that can later be inputted into a simulation. Afterward, using real-world data, we will be able to create simulations that can predict the different properties associated with each metal. The main benefit of using a digital twin approach is that the technology being developed may be tested virtually on computer programs without building it physically. This enables us to detect problems in advance which in turn significantly reduces manufacturing costs. The introduction of digital twins has also helped corporations grow while limiting their environmental footprint. For example, aircraft companies are continuously testing new materials that might improve efficiency. However, using trial and error to find the most appropriate material has proven to be time-consuming and involves a vast amounts of waste. To address this problem, digital twin programs can be used to model the materials and thus allowing the designers to choose the most suitable material.

4.2. 3D scanner

As previously mentioned, to create a digital twin, a 3D scanner must be used to scan the metals. For the purpose of this project, the scanner being used is the EinScan-SE, as shown in figure 2. This scanner is considered to be a low cost desktop scanner developed by the Chinese manufacturer Shining3D. It uses structured light technology to accurately measure the three-dimensional shape of an object using a light source and a camera system. The light source projects a stripe pattern of light onto the object and depending on the shape of the object, a distorted light pattern is produced that is captured by the camera. To ensure that all points of the object are scanned, the device includes an automatic turntable that continuously rotates the object until all points are scanned. The distance of each point on the object is then calculated using a method known as triangulation. Subsequently, a range map is produced which is used to create the final 3D model. Unlike laser scanners where a laser line is used, a structured light scanner uses blue or white light. As a result, it is crucial to eliminate any external light source as it may interfere with the final results. To avoid this issue during this study, a screening box was used to cover the scanner and the object to ensure that the scanner was shielded from any light from the surrounding.

Figure 2. 3D scanner along with the cardboard shield set-up.

Prior to starting, the scanner software offers the user the choice to either use a texture or non-texture scan. For the purposes of this project, a non-texture scan is sufficient. To begin, the object is placed on the turntable and the scanning process initiates. During the scanning process, the software enables the user to choose the number of turntable steps and the speed at which the turntable rotates. This provides us with greater flexibility as some of the shapes that were scanned required a certain modified turntable setting to allow all faces of the shape to be scanned accurately. For example, for larger shapes the turntable steps were increased to ensure that the scans were captured from all angles to provide a complete data set. Another important feature of the scanner is the ability to choose the mode of alignment which depends on the shape of the object being scanned. For this project, feature alignment was used which essentially means that the surface features are used as reference points and are continuously scanned as the turntable rotates. The software then calculates the distance between the position of the camera and the turntable and matches the scans to form a complete model of the object (Lapshin, R., 2004). An important note to keep in mind is that this type of alignment only works for non-symmetric shapes

and therefore a different mode of alignment must be chosen if a symmetric shape is being scanned such as a sphere. After the alignment is completed, the mesh can now be selected as either a watertight or an unwatertight model, depending on the application. In some cases, the scanned model may have some unfilled holes in it and it is referred to as a leaky model. When this happens, the simulation is able to stitch the surfaces together to make sure that all the holes are filled, and the model is transformed into a watertight model. In our case, Maxwell rejected models that were not completely enclosed. Hence, in this project, the watertight model was selected to examine in order to improve accuracy of the results. Next, we must choose the level of detail. The recommended detail level is medium as choosing the high detail option may result in a large file that the may not be able to handle in some cases. To reduce the file size and the number of triangles in the mesh, the user can use the simplification feature within the software.

Figure 3. Original model before simplification.

Figure 4. Modified model after simplification.

Figure 4 has been simplified by a simplification ratio of 30% when compared to Figure 3. It is difficult to spot any difference between the two figures by simply looking at them as the level of detail is similar in both. However, the file size and number of triangles has been significantly reduced in figure 4. The STL file size decreased from 28.73 MB in the original model to 8.62 MB in the simplified model. The number of triangles decreased as well from 598,614 triangles in the original model to 179,584 triangles in the simplified model.

Lastly, when exporting the model, it can be saved in one of the following formats: STL, PLY, OBJ, 3MF, or ASC. None of the mentioned files can be imported onto the Maxwell software, therefore; an intermediary software must be used. In this project a 3D computer-aided design modelling application known as FreeCAD was used to convert the scanned model from an STL file into a STEP file that is supported by Maxwell.

4.3. Ansys Maxwell

Ansys Maxwell is the electromagnetic field simulation software chosen to analyse and design the different experiments that were carried. Not only is the interface user-friendly, but it is also readily available across the university's computers. At the launch of this experimentation process,

the first step was to draw a semi-circle in 2D that was experiencing a magnetic field from a circle nearby which acted as a coil with current flowing inside it. In order to understand the characteristics and behaviour of the metal under test, it is crucial to understand what happens during the simulation process and how the software solves the electromagnetic fields.

4.3.1. Finite element method (FEM)

Maxwell uses a numerical method known as finite element method (FEM) to solve magnetic fields by converting a set of differential equations with certain boundary conditions to a system of linear equations that can be solved by the computer. During FEM, the problem, which in this case is the metal object, is divided into smaller pieces in a process known as meshing. These smaller pieces are now separated into elements and calculations are performed on each element. The elements take different shapes depending on the application but they are usually represented as triangles in 2D and tetrahedra in 3D. The size of the elements also varies depending on its distance from the object as seen in figure 6. The principle behind the FEM is to approximate a function $\mathbf{u}$ using a combination of basis functions as follows:

$$u_h = \sum_i^N u_i \psi_i \,, \tag{4}$$

Where u_h is the approximation of u, N is the number of nodes which in the case of a triangle represents its three vertices, and ψ_i denotes the basis functions.

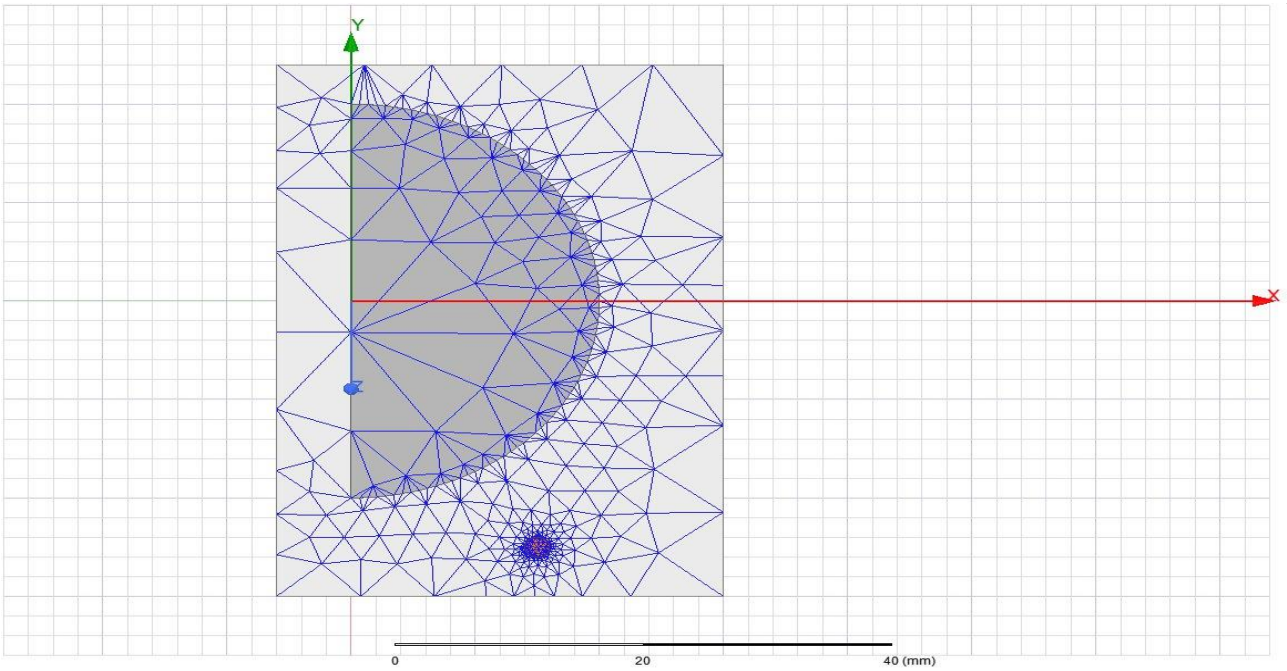

Figure 5. Representation of the mesh associated with the model.

An important feature of FEM is discretization. This refers to the element size used to obtain the required resolution. For example, near the boundary of the object, smaller elements are usually used as the rate of variation increases at the fastest rate where the magnetic field is strongest. Consequently, by using smaller elements the solver will provide greater accuracy. Nonetheless, this increased accuracy will result in increased computational cost. It is important to reach an equilibrium where the speed of the simulation is acceptable while still providing the required accuracy.

4.3.2. 2D model construction

Figure 6. 2D model of sphere and coil.

As previously explained, after drawing the semi-circle and circular coil, the materials for both the semi-circle and coil are assigned. Both the semi-circle and coil are cross sections which, when rotated about the y-axis, produce a sphere and a torus ring. The coil was assigned as a perfect electric conductor (PEC). This does not exist in nature but was used to observe the full effect of the magnetic field on the metal being tested. The semi-circle was assigned different materials to observe the changes that result as the material is changed. The first experiment was carried out

using aluminium and a magnetic induction spectrum was extracted from the impedance plot at various frequencies.

After assigning the materials and setting the boundary, the impedance against various frequencies is plotted in Maxwell and the resulting plot is exported to Excel for further manipulation. As discussed, the total impedance is divided by the frequency to produce the real and imaginary parts of the mutual inductance which are later plotted to produce the final version of the magnetic induction spectrum. However, before this is done it is important to isolate the metal that is being tested. The impedance plot that is provided by the software contains the total impedance which means that it consists of background values from the coil that need to be subtracted from the total impedance Z_T to get the results of the metal alone. This is done by assigning the semi-circle as vacuum, resulting in zero conductivity, instead of aliminium and running the simulation again using the same mesh that was used originally. To ensure that the same mesh is used the number of passes in the setup section of the software is changed to make the simulation run only once to ensure that the mesh does not change. A new impedance plot $Z_{T'}$ is then plotted which consists of the resistance and impedance associated with the coil alone. Finally, the new impedance $Z_{T'}$ is subtracted from the original one Z_T and the resulting impedance $Z_O$is that of the metal object alone which is then divided by the respective frequencies to produce the magnetic induction spectrum plotted on a log scale. The same procedures were then repeated for different materials of metals and the resulting differences in the plots were observed.

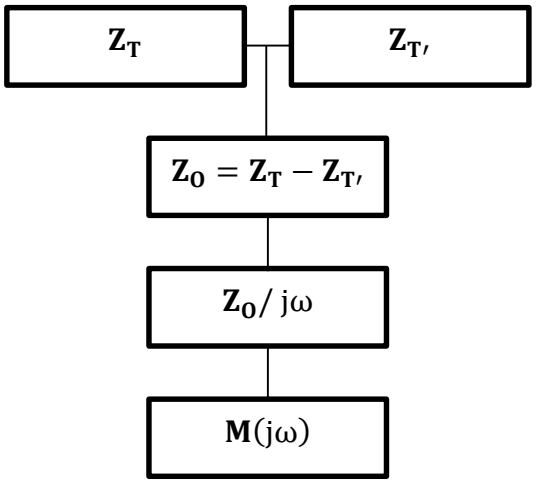

Figure 7. Flowchart to obtain magnetic induction spectrum from impedance.

4.3.3. 3D model construction

As seen in Figure 8, the model that was first constructed in 2D has now become a full sphere with

a torus ring that represents the coil. The same procedures that were used in the 2D were applied in 3D to verify that the model is consistent and yields the same results in both dimensions. Ultimately, two cast aluminium test metals were scanned using the 3D scanner and imported onto Maxwell to perform the necessary tests to ensure that the system we have developed is functioning properly.

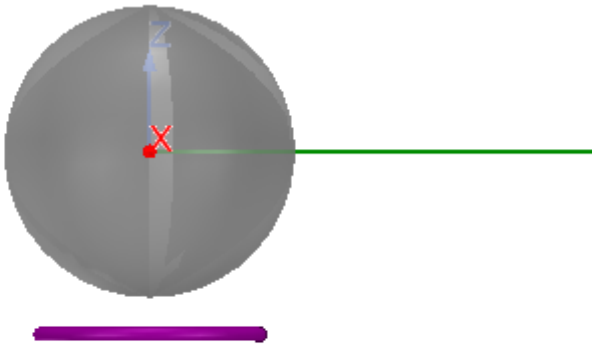

Figure 8. 3D representation of the 2D spherical model.

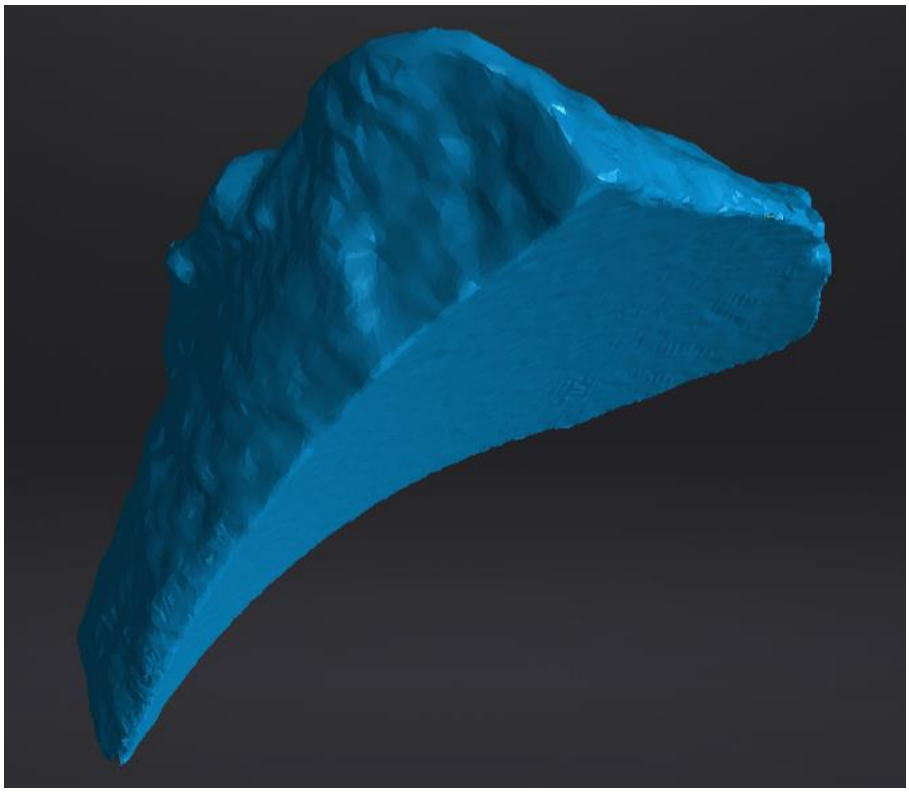

Figure 9. Top view 3D scan of metal 1.

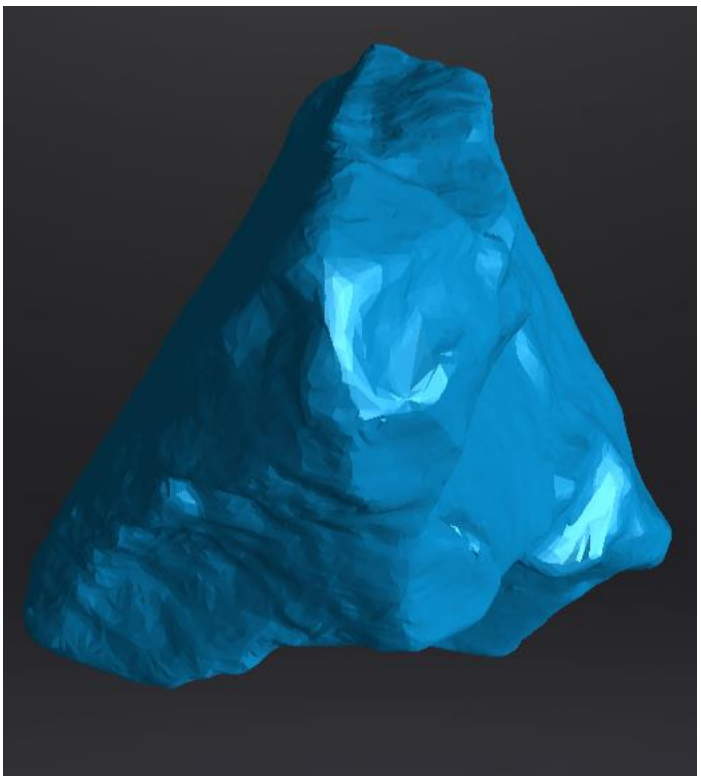

Figure 10. Top view 3D scan of metal 2.

Data on each metal piece was collected using the following procedure: the metal piece was placed properly on the turntable of the 3D scanner ensuring that the metal does not move as the turntable rotates and specific turntable setting were chosen depending on the size and shape of the metal. The scanner then starts scanning and a mesh of the metal is produced. Due to the placement of the metal on the turntable, the cameras of the scanner were not able to capture the bottom side of the metal and therefore the scanner software did not formulate any mesh on the base. This problem was solved by allowing the software to produce a watertight model that enclosed the bottom of the metal piece. The mesh is then exported onto Maxwell where a current carrying coil that acts as part of the MIS system exposes the metal piece to a magnetic field. The magnetic induction graph is then plotted using the same procedures that were mentioned previously and the results are compared to a data set that was obtained using the MetalID sensor.

The MetalID sensor was developed by O'Toole and J. Peyton at The University of Manchester to measure the magnetic induction spectra of metal scrap fragments (D. O'Toole, M. and J. Peyton, A., 2019). Metal 1 and Metal 2 were measured by PhD student Kane Williams. The metal pieces are first scanned by placing the metals 3 mm above the sensor and in a central position as shown in figure 11, but as with the simulation the scans will contain background noise and measurements from ferrite. Ferrite is used to calibrate the solenoid arrays within the sensor to remove any phase

shift that may occur in the system. Hence, the background and ferrite must also be measured and subtracted from the metal scan. The magnetic induction spectra for both metals are then plotted using the following equation:

$$\frac{\text{Metal scan} - \text{background scan}}{\text{Ferrite scan} - \text{background scan}}, \quad (5)$$

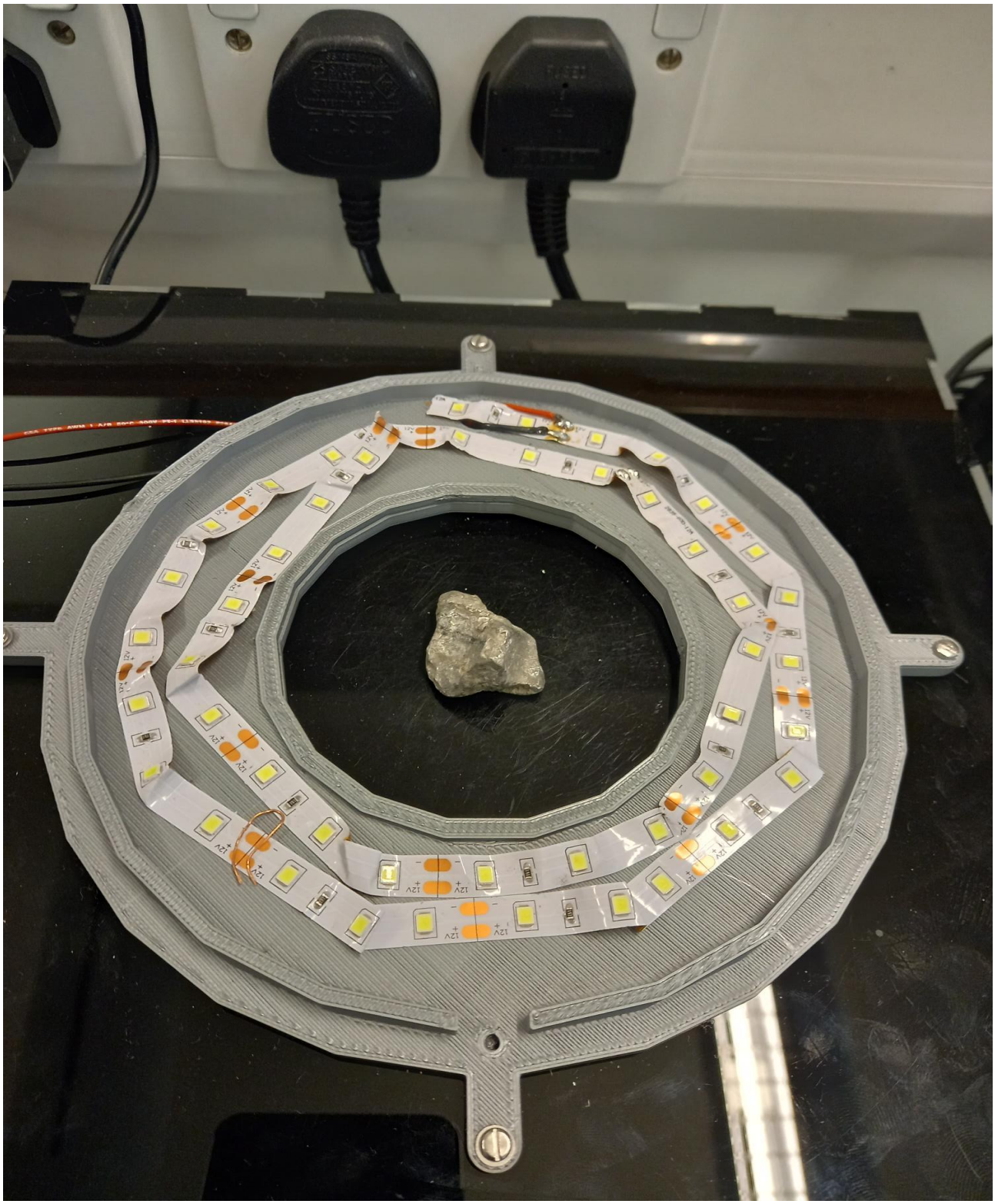

Figure 11. MetalID system with metal 2 placed in the center.

In an effort to get the most accurate results from Maxwell, the MetalID system and the same procedures were replicated in the simulation. The metal piece was placed in a central position 3 mm above a torus ring which represented the coil of the MetalID system. For this experiment the materials assigned were quite different than in the previous experiments as it was now being compared with results obtained from real life objects. Therefore, the metal was assigned as cast aluminium (AL-384) with a conductivity equivalent to 28% ICAS. The coil was assigned as copper just as in the MetalID system and was drawn with a major radius of 15 mm and a minor radius of 1 mm resulting in a 14 mm thick wire. An additional measurement was introduced from the ferrite rod which had a length of 16 mm and a diameter of 5 mm.

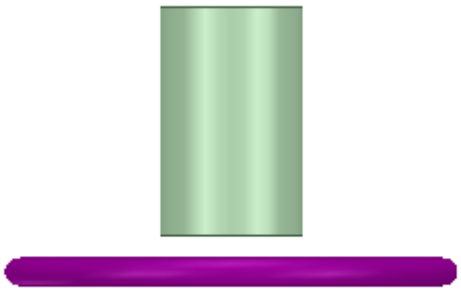

Figure 12. Representation of the ferrite rod in Maxwell.

4.4. Limitations

One of the main challenges faced during this research was the scanning process. The scanned metals contained at first more than 100,000 triangles in the mesh due to the edges and fringes in the shape of the metal. This required a great amount of detail to produce a scan that was almost identical to the real life shape of the metal. After exporting the scan onto Maxwell, the software was unable to solve the mesh as it was too complex and required a great amount of computational power. As a result, the mesh had to be simplified to a certain extent that allowed Maxwell to process and solve the model. To further elaborate on this, metal 2 initially contained about 500,000 triangles in its mesh. After the scanning phase, the mesh had to be simplified to eventually contain only 5,000 triangles. Triangle simplification reduces the sampling of the mesh by using algorithms that remove certain triangles that do not contribute significantly to the shape (Preim, B. and Botha, C., 2013). Such simplification reduces the processing time as the file size is reduced, but this comes at the cost of altering the original shape of the sample and reducing

accuracy.

Finally, as a low budget device, the EinScan-SE 3D scanner had some limitations that affected the results of this paper. For example, not all shapes could be scanned using the EinScan-SE scanner. However, for the purposes of this project, it was sufficient to introduce the idea of using MIS systems in scrap sorting to help encourage further development and investment and allow such systems to be used in industrial factories.

5. Results and discussion:

Key information can be extracted from the magnetic induction spectrum of a metal. The spectrum consists of the real and imaginary parts of the mutual inductance which when analysed provide crucial data concerning the metal under test. Both the real and imaginary parts of the mutual inductance are dependent on the size, material, and shape of the metal. The real and imaginary part is associated with the eddy currents that are produced as a result of the magnetic field that is induced. The imaginary component is a result of the conductive and magnetic properties of the metal (Davidson et al., 2018). In the case of a non-conducting object, the mutual inductance will consist of only the real component as the there are no resistive losses and therefore the total impedance Z_T will only contain the inductance of one of the coils.

5.1. 2D analysis

This section explores how different materials and sizes of a metal affect the magnetic induction spectrum of a given metal. All the metals used are non-magnetic metals as this paper focuses on using MIS for the purpose of sorting non-ferrous metals.

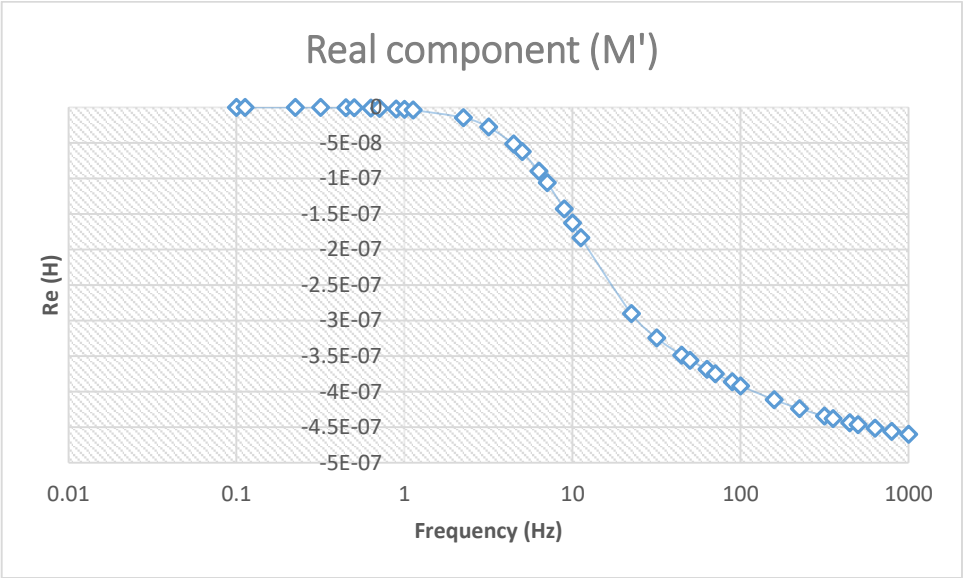

Figure 13. Real component of the spectral response of an aluminium sphere of radius 20 mm.

Figure 13 shows the typical real component of the magnetic induction spectrum for non-ferrous metals. The figure corroborates what was described in section 3 regarding the profile of the real component: It starts at zero and then forms a sigmoid to eventually converge towards an asymptote at around 1000 Hz. This convergence occurs as a result of the skin depth effect (O'Toole, M., Karimian, N. and Peyton, A., 2018). As the frequency increases, the eddy currents become concentrated near the surface of the metal and “penetration” is reduced. When this happens the real component is no longer affected by the conductivity since the eddy currents are only flowing near the surface of the metal.

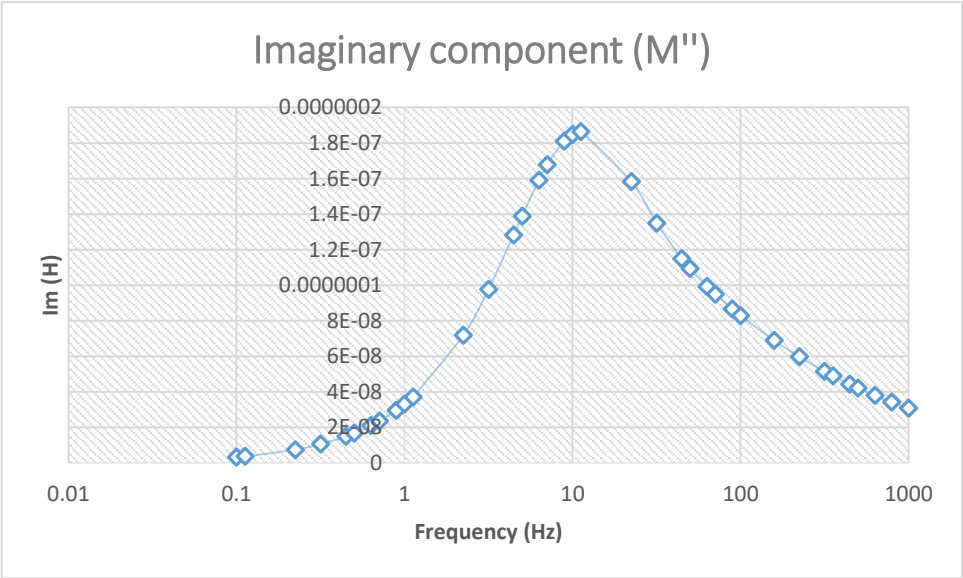

Figure 14. Imaginary component of the spectral response of an aluminium sphere of

radius 20 mm.

Figure 14 shows that the imaginary component starts at zero as we previously predicted and reaches a peak at around 10 Hz and eventually converges. The imaginary component represents the resistive response of the metal under test, therefore; it can be deduced from figure 14 that the resistive loss is highest at 10 Hz which suggests that the magnetic field interaction between the coil and metal piece reaches a maximum and then as the frequency increases the resistive loss decreases and converges due to the skin depth effect which results in the current flowing only near the surface of the metal as with the real component.

By observing figures 13 and 14, we can recognize that as the imaginary component reaches its peak the gradient of the real component, which is essentially the inductance, decreases as it has now reached a region whereby most of the current is accumulating near the surface of the metal resulting in a minimal change of current flow.

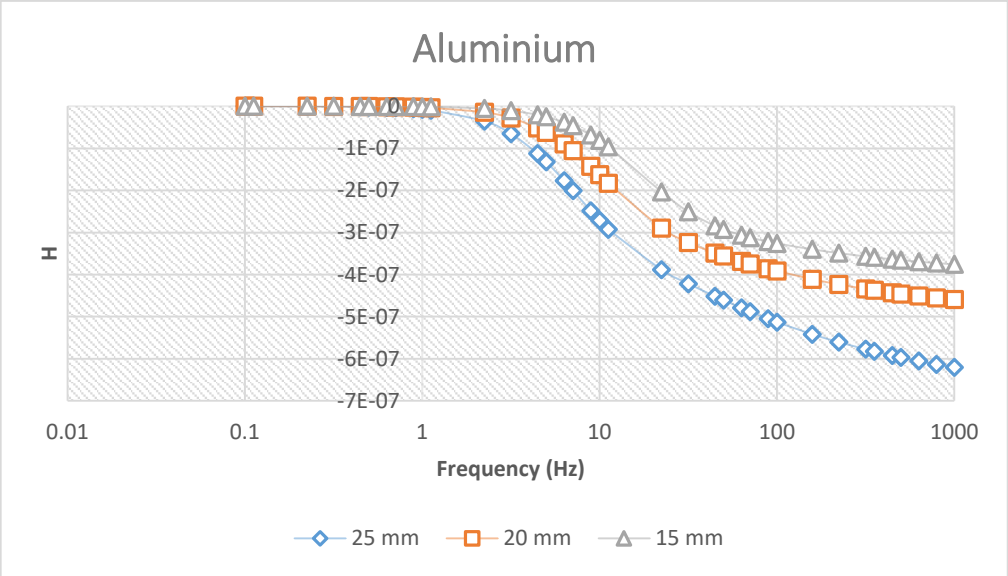

Figure 15. The variance in the spectroscopic real component with a change in object size.

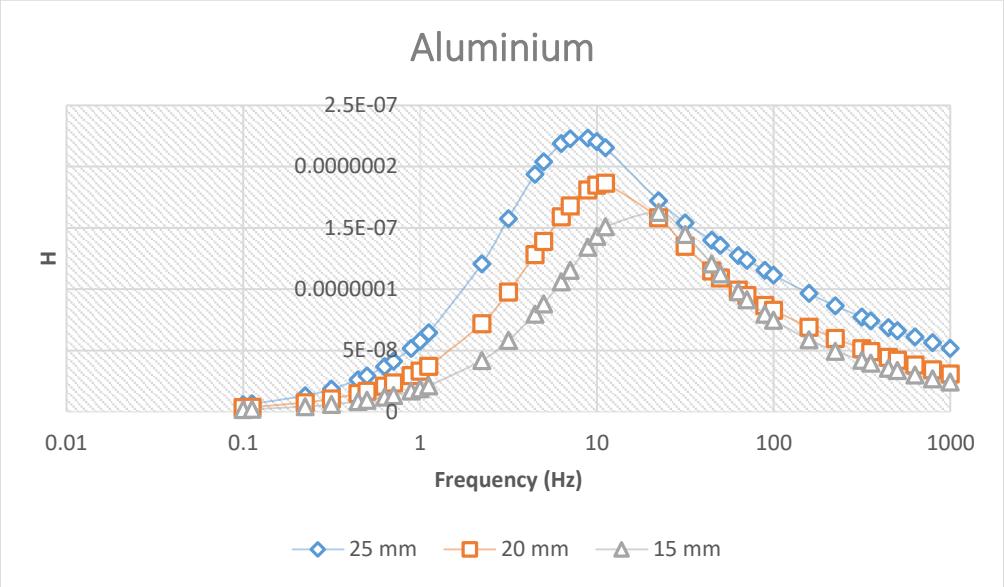

Figure 16. The variance in the spectroscopic imaginary component with a change in object size.

Figures 15 and 16 show that the real and imaginary components of the mutual inductance are indeed dependent on the size of the object. The metals in the figures are all made from the same material (Aluminium) and have the same shape (spherical). The only difference is the diameter of the sphere which varies from 15 mm to 25 mm. The real components all start from zero; however, the gradient of the curves varies as the frequency increases. The metal piece that is largest in size (25 mm) exhibits the sharpest gradient. Also, the values to which the curves converge varies with the largest piece having the largest absolute converging point between the three different sizes of the metal.

As for the imaginary component, by observing figure 16 it becomes evident that as the size of the metal increases the frequency at which the imaginary component peaks tends to shift to a lower frequency. Also, the metal piece with the largest diameter seems to have the largest peak value. All these changes occur as a result of the increased size which results in increased interaction between the metal piece and the surrounding magnetic field which in turn impacts the magnitude and direction of the generated eddy currents (Abdel-Rehim et al., 2016).

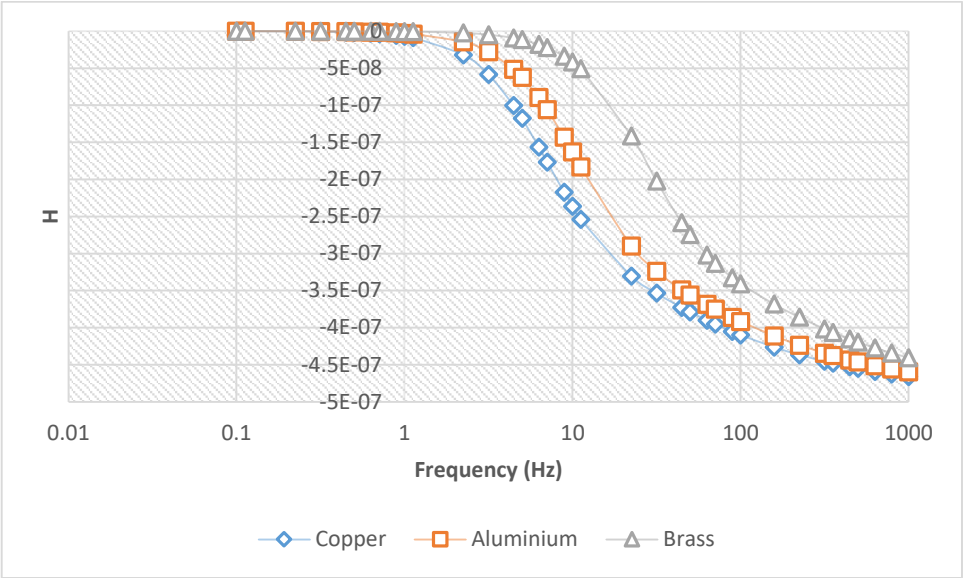

Figure 17. The variance in the spectroscopic real component with a change in object material.

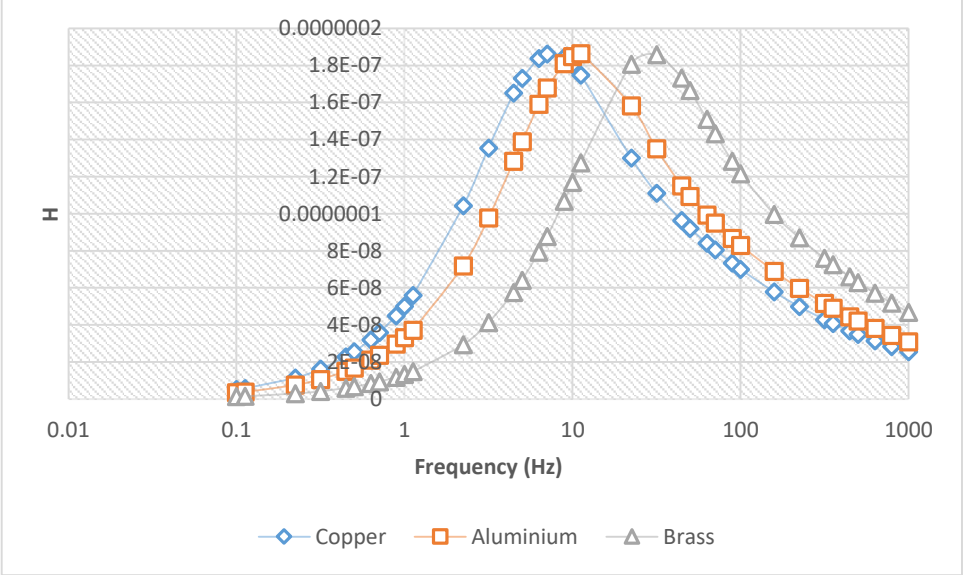

Figure 18. The variance in the spectroscopic imaginary component with a change in object material.

It is important to be able to differentiate between the different materials of non-ferrous metals by analysing their respective magnetic induction spectra. In figures 17 and 18, the spectroscopic properties of copper, aluminium, and brass are compared with one another. All the materials are simulated using the same drawing which includes a sphere of diameter 20 mm that is 5 mm away from a circular coil. Each material has a unique curve due to the different properties, such as conductivity, associated with each material. As shown in figure 17, the real component for all three materials will eventually converge to the same value as the frequency increases; however,

the main difference between the three curves is the gradient. As the electrical conductivity of the material increases, the gradient becomes sharper. This can be proven by observing figure 17 which shows that copper has the sharpest gradient as it has the highest conductivity between the three metals.

In the case of the imaginary component, it seems like all three metals have almost the same peak value. Therefore, the metals can be differentiated by recording the frequency at which each metals peaks. As shown in figure 18, the metal with higher conductivity tends to peak at a lower frequency when compared with another metal of lower conductivity. In figure 18, copper peaks at the lowest frequency followed by aluminium and brass, respectively. This is in accordance with their respective electrical conductivities. The changes described in the real and imaginary components occur due to the difference in electrical conductivity which contributes to the skin depth associated with the conductor. As the electrical conductivity increases the skin depth decreases due to the inverse relationship between the skin depth and conductivity which is explained by the following:

$$\delta = \sqrt{\frac{\rho}{\pi f \mu_o \mu_r}}, \tag{6}$$

Where δ is the skin depth, ρ is the resistivity of the conductor, f is the frequency, μ_o is the permeability of free space, and μ_r is the relative magnetic permeability of the conductor.

5.2. 3D analysis

Before inserting the metal pieces that were scanned into the 3D modeller, the model that was simulated in 2D was replicated and simulated again in 3D to verify that the 2D and 3D results are in agreement. It is important to note that the results were not identical and the differences between the 2D and 3D results amounted to more than 10%.

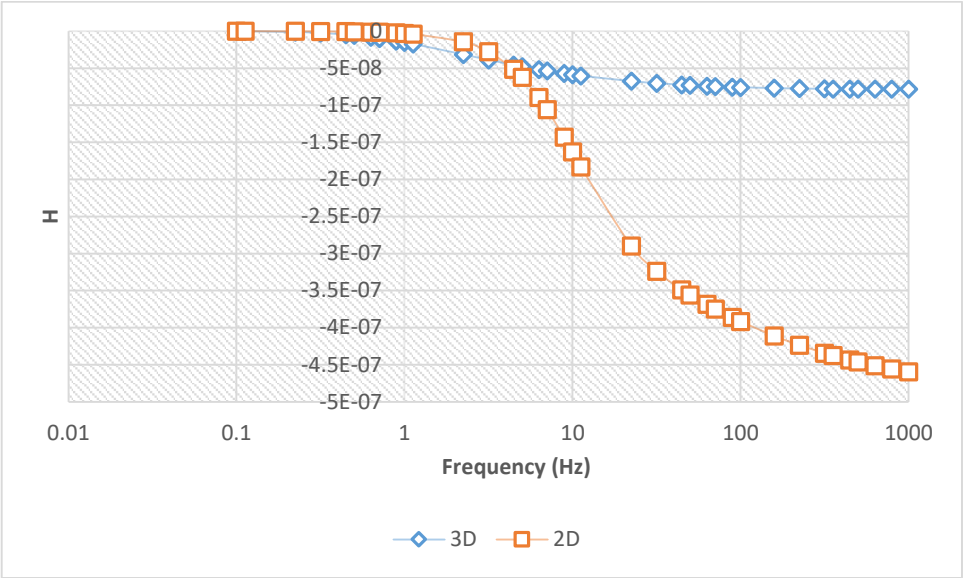

Figure 19. Spectroscopic real component in 2D and 3D.

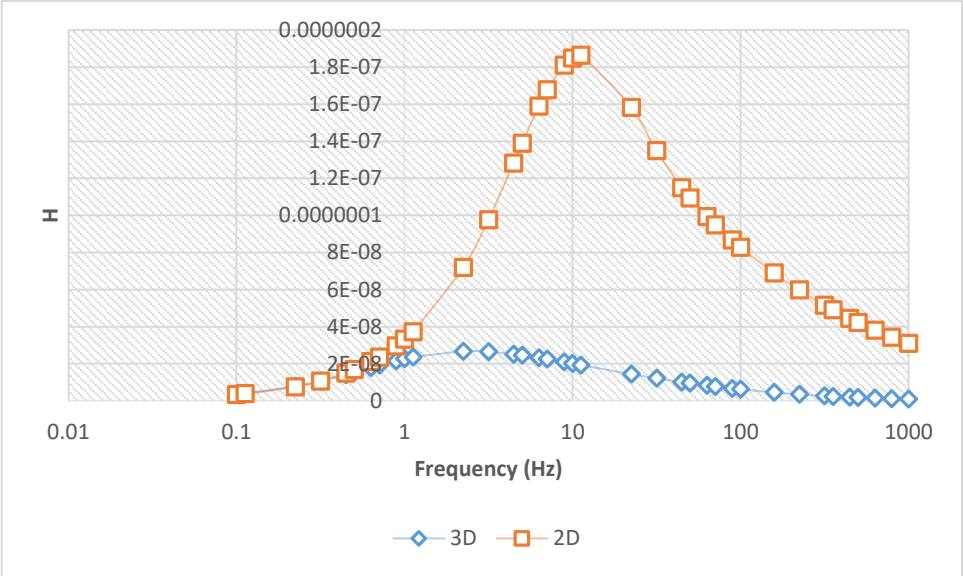

Figure 20. Spectroscopic imaginary component in 2D and 3D.

There is a clear discrepancy between the 2D and 3D results for both the real and imaginary components. Generally, the simulated results do not agree with the experimentally derived results due to the simulation's inability to reproduce the same physical and electrical properties as in the real world. However, this does not usually yield an error equivalent to the one observed in figures 19 and 20 which suggests that there may be some additional error involved. The differences in the magnitudes of the real component in 2D and 3D suggest that a difference in permeability may be the source of error. Also, the imaginary component in 3D appears to peak at a lower frequency when compared to the 2D which suggests that there might be an error in the dimensions of one of the models. For example, the sphere that was drawn in 3D might have a larger diameter which

explains why it peaks at a lower frequency.

5.2.1. Metal 2 3D analysis

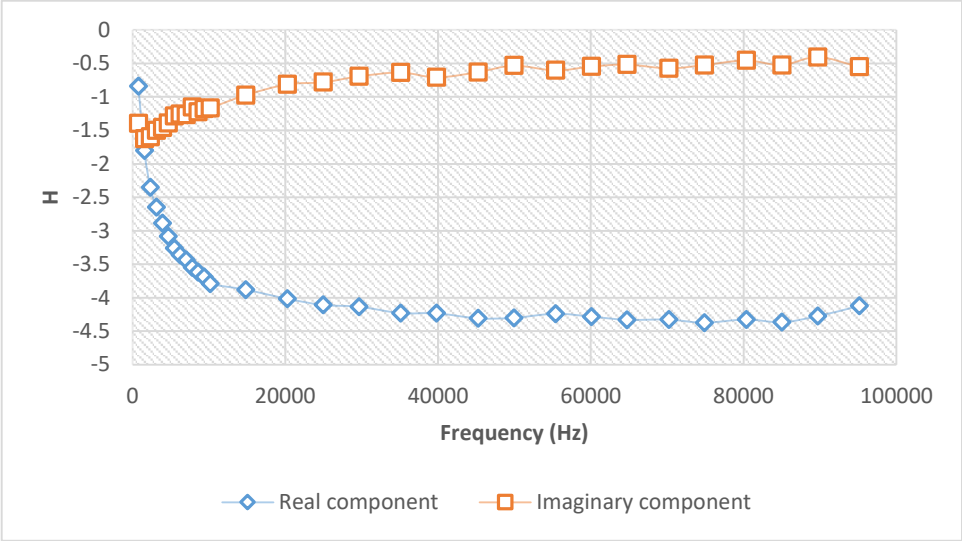

Figure 21. Magnetic induction spectrum of metal 2 produced by the MetalID.

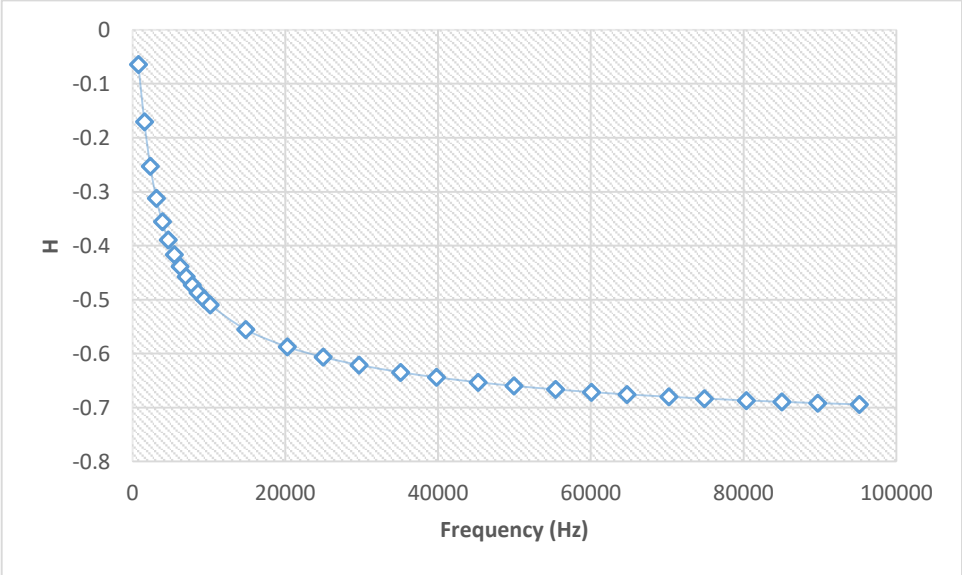

Figure 22. Real component of magnetic induction spectrum of metal 2 produced by the computer simulation.

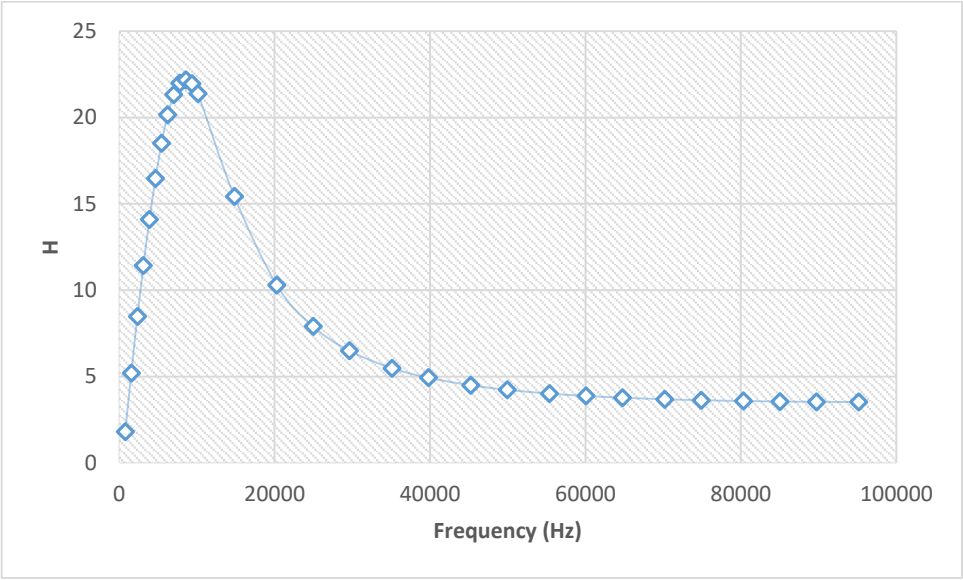

Figure 23. Imaginary component of magnetic induction spectrum of metal 2 produced by the computer simulation.

There is a clear difference between the simulated and measured results. However, this difference was expected since the simulated environment is not exactly the same as real life. The shapes and trends of the curves suggest that with further research and by making the simulation as close as possible to the real life environment the difference between simulated and measured results will get reduced. It is important to note that the orientation of the metal piece plays a role in the shape of the curves. In this case, it was unknown how exactly the metal piece was scanned when placed on the sensor, therefore; this might be one of the sources of error. Also, the electrical specification of the MetalID such as current and voltage might have played a role in the error produced.

6. Conclusion and further work

After testing different materials of non-ferrous metals and different sizes, it was concluded that with further research and investment MIS may soon be deployed at a large scale in industrial factories to help sort the different types of metals. The results in 2D were sufficient and could be easily analysed. Whereas, this was not the case for the 3D modelling which involved some errors that affected the outcome. Unfortunately, there was not enough time to investigate and correct the errors involved. Nonetheless, the shapes and trends of the curves in 3D matched those in 2D which meant that with further research and development the appropriate results may be obtained.

Although the research on MIS based systems has shown promising results, there still remains some challenges. The recovery rate associated with such systems may be substantially improved by adding a shape scanner and colour sensor to the initial system whereby allowing the device to examine a combination of the metal's characteristics resulting in a more accurate identification.

7. References

1. Internal Market, Industry, Entrepreneurship and SMEs. 2021. Non-ferrous metals. [online] Available at: <https://ec.europa.eu/growth/sectors/raw-materials/related-industries/metal-industries/non-ferrous-metals_fi> [Accessed 21 November 2021].
2. Beason, J., 2019. How to Recycle Ferrous and Non-Ferrous Metals | Rubicon. [online] Rubicon. Available at: <https://www.rubicon.com/blog/ferrous-and-non-ferrous-metals/> [Accessed 21 November 2021].
3. Russo, R., Mao, X., Liu, H., Yoo, J., Mao, S., 1990. Time-resolved plasma diagnostics and mass removal during single-pulse laser ablation. [online] pp.1-2. Available at: <https://link.springer.com/article/10.1007/s003390051553> [Accessed 21 November 2021].
4. Olympus-ims. n.d. Scrap Recycling with XRF – Sort More, Sort Faster, and Increase Your Profits. [online] Available at: <https://www.olympus-ims.com/en/applications/scrap-recycling-xrf-sort/> [Accessed 21 November 2021].
5. O'Toole, M., Marsh, L., Davidson, J., Tan, Y., Armitage, D. and Peyton, A., 2015. Non-contact multi-frequency magnetic induction spectroscopy system for industrial-scale bio-impedance measurement. pp.5-9.
6. Van Heusden, R., Harry, M. and Puleo, M., 2020. Why addressing the aluminium industry's carbon footprint is key to climate action. [online] World Economic Forum. Available at: <https://www.weforum.org/agenda/2020/11/the-aluminium-industry-s-carbon-footprint-is-higher-than-most-consumers-expect-heres-what-we-must-do-next/> [Accessed 30 February 2022].
7. Office for National Statistics (UK). (2021). Carbon dioxide (CO2) emissions from the production of aluminum in the United Kingdom* from 1990 to 2019 (in 1,000 metric tons). Statista. Statista Inc.. Accessed: March 30, 2022. https://www.statista.com/statistics/485975/co2-emissions-from-the-aluminum-production-uk/.
8. Climate Change Committee, 2021. Progress in reducing emissions. [online] pp.19-20. Available at: <http://www.theccc.org.uk/publications> [Accessed 17 February 2022].
9. NMSC. (2022). Global battery electric vehicle market size forecast 2030. Statista. Statista Inc.. Accessed: March 30, 2022. https://www.statista.com/statistics/1254513/battery-electric-vehicle-market-size-forecast/.
10. Copper Development Association, 2022. HOW COPPER DRIVES ELECTRIC VEHICLES. [image] Available at: <(https://www.copper.org/publications/pub_list/pdf/A6192_ElectricVehicles-Infographic.pdf> [Accessed 30 February 2022].
11. Arrobas, D., Hund, K., Mccormick, M., Ningthoujam, J. and Drexhage, J., 2017. The Growing Role of Minerals and Metals for a Low Carbon Future. [online] pp.26-27. Available at: <https://documents.worldbank.org/en/publication/documents-reports/documentdetail/207371500386458722/the-growing-role-of-minerals-and-metals-for-a-low-carbon-future> [Accessed 15 February 2022].

12. Tykot, R., 2016. Using Nondestructive Portable X-ray Fluorescence Spectrometers on Stone, Ceramics, Metals, and Other Materials in Museums: Advantages and Limitations. Applied Spectroscopy, 70(1), p.43.
13. Dingley, G. and Soleimani, M., 2021. Multi-Frequency Magnetic Induction Tomography System and Algorithm for Imaging Metallic Objects. Sensors, [online] 21(11), p.3. Available at: <https://www.mdpi.com/1424-8220/21/11/3671/htm> [Accessed 7 February 2022].
14. D. O'Toole, M. and J. Peyton, A., 2019. Classification of Non-ferrous Scrap Metal using Two Component Magnetic Induction Spectroscopy. IEEE, [online] p.2. Available at: <https://ieeexplore.ieee.org/abstract/document/8706104> [Accessed 19 February 2022].
15. Lapshin, R., 2004. Feature-oriented scanning methodology for probe microscopy and nanotechnology. Nanotechnology, [online] 15(9), pp.1135-1137. Available at: <http://www.lapshin.fast-page.org/publications/R.%20V.%20Lapshin,%20Feature-oriented%20scanning%20methodology%20for%20probe%20microscopy%20and%20nanotechnology.pdf?i=1> [Accessed 25 March 2022].
16. Preim, B. and Botha, C., 2013. Visual Computing for Medicine. 2nd ed. Elsevier Science, pp.229-235.
17. O'Toole, M., Karimian, N. and Peyton, A., 2018. Classification of Nonferrous Metals Using Magnetic Induction Spectroscopy. IEEE Transactions on Industrial Informatics, 14(8), p.5.
18. Davidson, J., Abdel-Rehim, O., Hu, P., Marsh, L., O'Toole, M. and Peyton, A., 2018. On the magnetic polarizability tensor of US coinage. Measurement Science and Technology, 29(3), p.2.
19. Abdel-Rehim, O., Davidson, J., Marsh, L., O'Toole, M. and Peyton, A., 2016. Magnetic Polarizability Tensor Spectroscopy for Low Metal Anti-Personnel Mine Surrogates. IEEE Sensors Journal, 16(10), p.3777.